

Inter-calibration Results of the Advanced Microwave Scanning Radiometer-2 Over Ocean

Suleiman O. Alsweiss, *Member, IEEE*, Zorana Jelenak, *Member, IEEE*, Paul S. Chang, *Member, IEEE*, Jun Dong Park, *Senior Member, IEEE*, and Patrick Meyers

Abstract—In this paper, the oceanic radiometric calibration biases of the Advanced Microwave Scanning Radiometer-2 (AMSR2) onboard the Global Change Observation Mission-Water (GCOM-W1) are analyzed. The double difference (DD) approach is utilized to perform inter-sensor inter-calibration for AMSR2 with the Tropical Rainfall Measuring Mission (TRMM) Microwave Imager (TMI) as the reference radiometer. This technique utilizes radiative transfer model (RTM) simulations and near-simultaneous clear-sky ocean-only observed brightness temperatures from the two microwave radiometers to estimate and correct the radiometric biases of ocean scenes for AMSR2 on a channel by channel basis.

Index Terms—Advanced Microwave Scanning Radiometer-2 (AMSR2), double difference (DD), inter-calibration, ocean, Tropical Rainfall Measuring Mission (TRMM) Microwave Imager (TMI).

I. INTRODUCTION

PASSIVE microwave radiometry is a special application of microwave communications technology for the purpose of collecting Earth's electromagnetic radiation. With the use of radiometers onboard earth orbiting satellites, engineers and scientists are able to monitor the Earth's environment and climate system on both short- and long-term temporal scales with near global coverage (e.g., [1], [2]). Therefore, having well calibrated and stable microwave radiometers can provide unprecedented data to the scientific community for weather and climate research and operational activities.

The initial postlaunch radiometer calibration and validation (Cal/Val) efforts commenced with the launch of the first Special Sensor Microwave Imager (SSM/I) on the Defense Meteorological Satellite Program (DMSP F-8) in 1987 [3] followed by a series of similar instruments (F-10 to F-15). The Naval Research Laboratory (NRL) led these Cal/Val activities aiming to study the stability of these instruments and their geolocation accuracy [4]–[6]. The identical design of the SSM/I instruments provides a unique opportunity to directly compare near simultaneous observations from corresponding channels.

Manuscript received February 18, 2014; revised April 07, 2014; accepted June 05, 2014. Date of publication June 30, 2014; date of current version December 21, 2015.

The views expressed in this paper are those of the authors and must not be interpreted as those of National Oceanic and Atmospheric Administration or the U.S. Government.

The authors are with the Center for Satellite Applications and Research (STAR), National Environmental Satellite, Data, and Information Service (NESDIS), National Oceanic and Atmospheric Administration (NOAA), College Park, MD 20740 USA (e-mail: suleiman.alsweiss@noaa.gov).

Color versions of one or more of the figures in this paper are available online at <http://ieeexplore.ieee.org>.

Digital Object Identifier 10.1109/JSTARS.2014.2330980

These inter-calibration efforts, started 25 years ago, continue to be exploited to calibrate other spaceborne radiometers including the six SSM/I [7], two Special Sensor Microwave Imager/Sounder (SSMIS) [8], Tropical Rainfall Measuring Mission (TRMM) Microwave Imager (TMI) [9], the Advanced Microwave Scanning Radiometer for the Earth Observing System (AMSR-E) [10], and the most recently the Global Precipitation Measurement (GPM) mission [11].

In May 2012, the Japanese Aerospace Exploration Agency (JAXA) successfully launched the Global Change Observation Mission-Water (GCOM-W1) with the Advanced Microwave Scanning Radiometer-2 (AMSR2) onboard. The observed brightness temperatures (Tbs) from AMSR2 will be used to infer several geophysical parameters over land and ocean. Thus, well calibrated AMSR2 Tbs will significantly improve the performance and accuracy of the geophysical retrieval algorithms and reduce retrievals errors.

With our main immediate goal to generate oceanic environmental data records (EDRs) using AMSR2 observed Tbs (i.e., sea surface temperature, sea surface wind speed, cloud liquid water, and total precipitable water); the scope of this paper will focus on identifying and correcting residual calibration biases in AMSR2 Tbs over ocean scenes with respect to TMI. We started with describing the instruments and datasets used in this study in Section II, then the inter-calibration methodology, followed by results in Sections III and IV, respectively. In Section V, AMSR2 stability was evaluated, and conclusion is presented in Section VI.

II. INSTRUMENTS DESCRIPTION

Inter-calibration between sensors relies on finding collocated Tb measurements between different platforms. For sun-synchronous orbits, these points occur only at high latitudes near the poles [8], which greatly limit the amount of available data for inter-calibration. Thus, for a sun-synchronous radiometer like AMSR2 (local time of ascending node 13:30), a nonsun-synchronous, low inclination orbiter will create a larger amount of collocated observations to be used in the analysis. Hence, TMI was chosen as the reference radiometer to study the calibration biases of AMSR2. In Sections II-A and II-B, some necessary background on the instruments design specifications for both AMSR2 and TMI are provided.

A. AMSR2

The GCOM program is part of JAXA's broader commitment toward global and long-term observation of the Earth's

TABLE I
AMSR2 INSTRUMENT SPECIFICATIONS

Center freq. (GHz)	Band width (MHz)	Beam width (3 dB, deg.)	Ground IFOV (km)	Sampling interval (km)
6.925/7.3	350	1.8	35 × 62	10
10.65	100	1.2	24 × 42	
18.7	200	0.65	14 × 22	
23.8	400	0.75	15 × 26	
36.5	1000	0.35	7 × 12	
89.0	3000	0.15	3 × 5	5

environment. GCOM consists of two medium-size, polar-orbiting satellite series with 1-year overlap between them for inter-calibration. The two satellite series are GCOM-W (Water) and GCOM-C (Climate). Two instruments were selected as payloads for these missions to cover a wide range of geophysical parameters: AMSR2 on GCOM-W and the Second-Generation Global Imager (SGLI) on GCOM-C. The AMSR2 instrument will perform observations related to the global water and energy cycle, whereas the SGLI will conduct surface and atmospheric measurements related to the carbon cycle and radiation budget [12].

The GCOM-W project is a 13-year mission with three satellites in series, each with a 5-year lifetime including a 1-year overlap with follow-on satellite for calibration purposes. The GCOM-W1, launched in May 2012, will be followed by the GCOM-W2, and GCOM-W3 nominally planned for launch in 2016, and 2020, respectively.

AMSR2 onboard GCOM-W1 is a microwave radiometer system that measures dual polarized [vertical (V-pol) and horizontal (H-pol)] radiances at 6.9, 7.3, 10.65, 18.7, 23.8, 36.5, and 89.0 GHz. It is a sun-synchronous orbiter that acquires microwave radiance data by conically scanning the Earth’s surface to obtain measurements along a semicircular pattern in front of the spacecraft. It operates at a nominal earth incidence angle (EIA) of 55° that results in a wide swath of 1450 km. The aperture diameter of AMSR2 antenna is 2.0 m with an instantaneous field of view (IFOV) spatial resolution that varies inversely with frequency [13].

AMSR2 inherited the most of AMSR-E characteristics with some important improvements including: a larger main reflector (compared to the 1.6 m diameter of AMSR-E), the addition of the 7.3 GHz channels (for C-band radio frequency interference (RFI) detection), 12-bit quantization for all channels, and improvements in the calibration system [14]. Summarized operating characteristics of AMSR2 are shown in Table I and the instrument design and geometry in Fig. 1.

B. TMI

TMI is a conically scanning total power microwave radiometer, launched onboard TRMM in November 1997 into a near circular nonsun-synchronous orbit at a 350-km altitude with an inclination of 35°. In August 2001, TMI underwent an orbital boost, with new operating altitude of 402.5 km, to increase its operational lifetime. Now, it acquires data from an azimuth arc of 130°, at 53.2° nominal EIA, resulting in an 878-km swath. It has a total of nine radiometer channels: four dual polarized (V- and H-pol) measurements at frequencies of 10.65, 19.35, 37, and 85.5 GHz, and a single polarization measurement (V-pol only) at

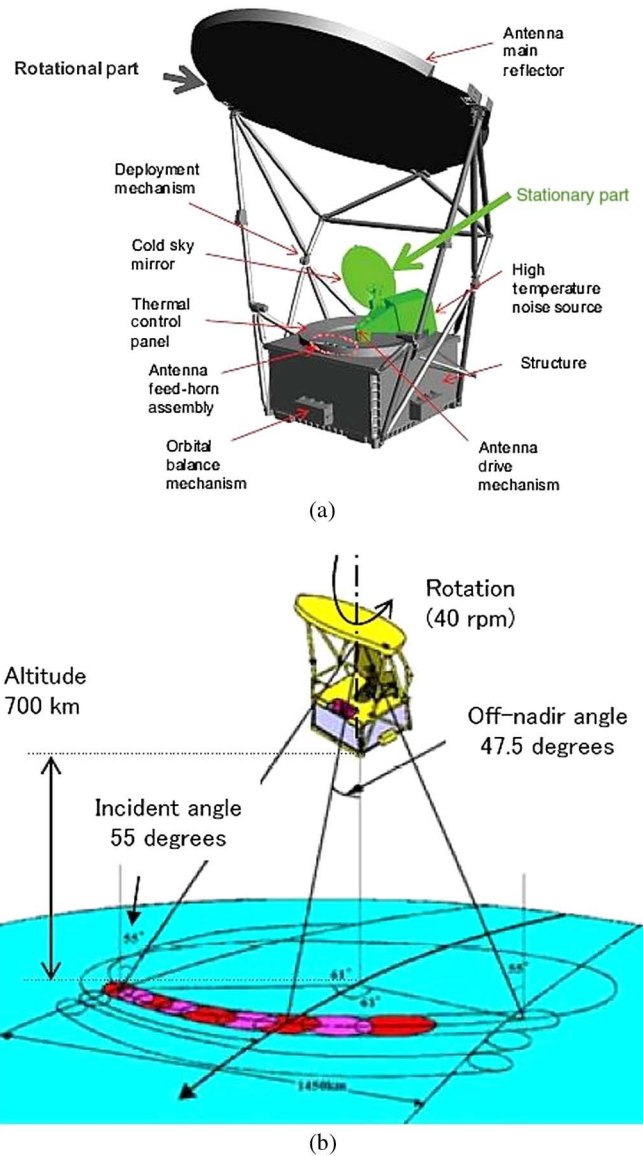


Fig. 1. Overview of AMSR2 (a) instrument design and (b) geometry (images credit: JAXA).

TABLE II
TMI INSTRUMENT SPECIFICATIONS

Center freq. (GHz)	Band width (MHz)	Polarization	Ground IFOV (km)
10.65	100	V/H	73 × 43
19.35	500	V/H	35 × 21
21.3	200	V	27 × 21
37.0	2000	V/H	19 × 10
85.5	3000	V/H	8 × 6

21.3 GHz. The spatial resolution for individual measurements varies from 6 km at 85.5 GHz channels to 43 km at 10.65 GHz channels as shown in Table II.

III. INTER-CALIBRATION METHODOLOGY

The inter-calibration methodology followed in this paper utilizes the well known double difference (*DD*) technique to

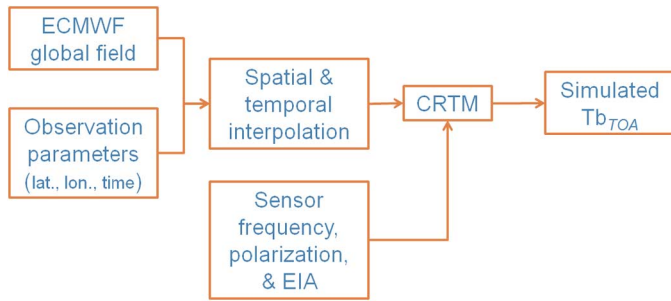


Fig. 2. Top of atmosphere brightness temperature (Tb_{TOA}) simulation block diagram.

provide a way to inter-calibrate two microwave radiometers. The main advantage of the *DD* method is that it accounts for center frequency, EIA, and orbital differences between instruments being inter-calibrated. To calculate *DD*, we need first to find the single difference (*SD*) for each radiometer, which is the difference between the observed and the simulated radiometer Tbs, with the latter generated using a radiative transfer model (RTM) and supplementary data.

A. Observed Brightness Temperatures

The AMSR2 data used in this study are JAXA's Level 1B version 1.1 (GW1AM2 L1B v1.1) released on March 1, 2013. In addition to observed Tbs, this data product contains the observation position (latitude, longitude), time, and orbit information. The product summary and description is available online at [15]. The major modifications from the version 1.0 Tbs can be summarized as [16]: the correction of cold sky antenna temperature for 6.9 and 7.3 GHz V- and H-pol channels, the correction of hot load Tbs for all channels, and the updated antenna pattern correction (APC) coefficient for all channels.

For TMI, the data used herein are version 7 (v7) of the Level 1B Calibrated Tb product (TMI 1B11). The product summary and description for TMI 1B11 can be found in the Goddard Earth Sciences Data and Information Services Center (GES DISC) Web page [17]. The TMI 1B11 has gone through multiple revisions and improvements over TRMM's lifetime with the most recent, v7, in 2011. One of the changes from v6 to v7 was the implementation of time-varying solar bias correction [18], [19]. This TMI data product is available for public and can be downloaded using the Mirador Earth Science Data Search Tool [20] developed at the GES DISC.

B. Simulated Brightness Temperatures

Modeling top-of-the-atmosphere brightness temperatures (Tb_{TOA}) using a microwave RTM is a key procedure in the calibration methodology implemented in this paper. For that purpose, we used the Joint Center for Satellite Data Assimilation (JCSDA) community RTM (CRTM) [21] version 2.1 with the Fast Microwave Ocean Emissivity Model (FASTEM) version 5.0 [22]. The CRTM consists of four main physical processes: the absorption of radiation by the gaseous constituents of the atmosphere, the absorption and scattering of radiation by clouds and aerosols, the surface emission of radiation and the surface interaction with downwelling atmospheric radiation. The result

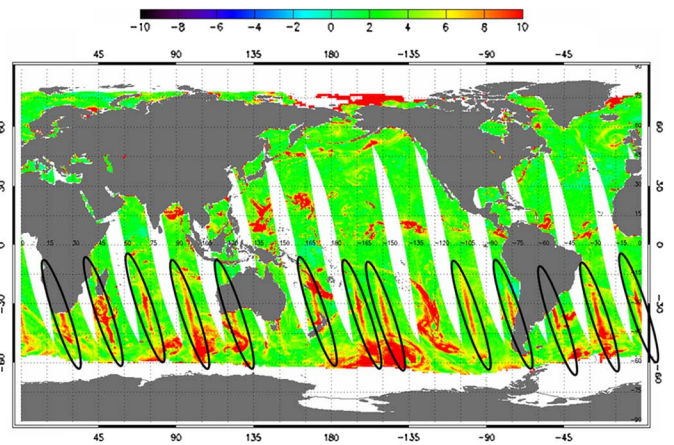


Fig. 3. Sun glitter effect on AMSR2 ascending orbits.

TABLE III
AMSR2/TMI MEAN DOUBLE DIFFERENCE

Channel	<i>DD</i> ascending (K)	<i>DD</i> descending (K)
10 GHz, V-pol	4.0	3.9
10 GHz, H-pol	4.6	4.7
18 GHz, V-pol	3.2	3.4
18 GHz, H-pol	1.8	1.9
23 GHz, V-pol	3.2	3.5
36 GHz, V-pol	3.5	3.6
36 GHz, H-pol	4.4	4.3
89a GHz, V-pol	1.1	1.1
89a GHz, H-pol	2.3	2.4
89b GHz, V-pol	0.7	0.8
89b GHz, H-pol	1.8	1.9

from the summation of these processes yields the simulated satellite sensor Tb_{TOA} .

To run the CRTM, we used the European Centre for Medium-Range Weather Forecasts (ECMWF) [23], [24]. These data are available every 6 h (03z, 09z, 15z, and 21z) at 0.25° latitude/longitude (lat/lon) grid composed of 1440×720 grid boxes. The surface environmental parameters provided in the data are: hybrid level 1 surface pressure, sea surface temperature, surface skin temperature, and 10-m U and V wind components. The atmospheric environmental parameters are provided in 91 pressure levels and are as follows: height profiles of pressure, temperature, specific humidity, O₃ mass mixing ratio, cloud ice water content, and cloud liquid water content.

ECMWF global fields were spatially and temporally interpolated to the sensor observation time and location. Afterward, the interpolated surface and atmospheric parameters are fed to the CRTM along with the instrument frequency, polarization, and EIA to simulate Tb_{TOA} . Fig. 2 shows a top-level block diagram for the simulation process used in this study.

C. Double Difference

The simplest and the most straightforward method for inter-calibration is the direct comparison of observed radiances from two radiometers. Unfortunately, even when the two radiometers being compared share the same center frequencies and nominal EIA, attitude control offset and different equatorial crossings will introduce different EIAs and diurnal variability. This might cause Tb differences that are not necessarily calibration errors.

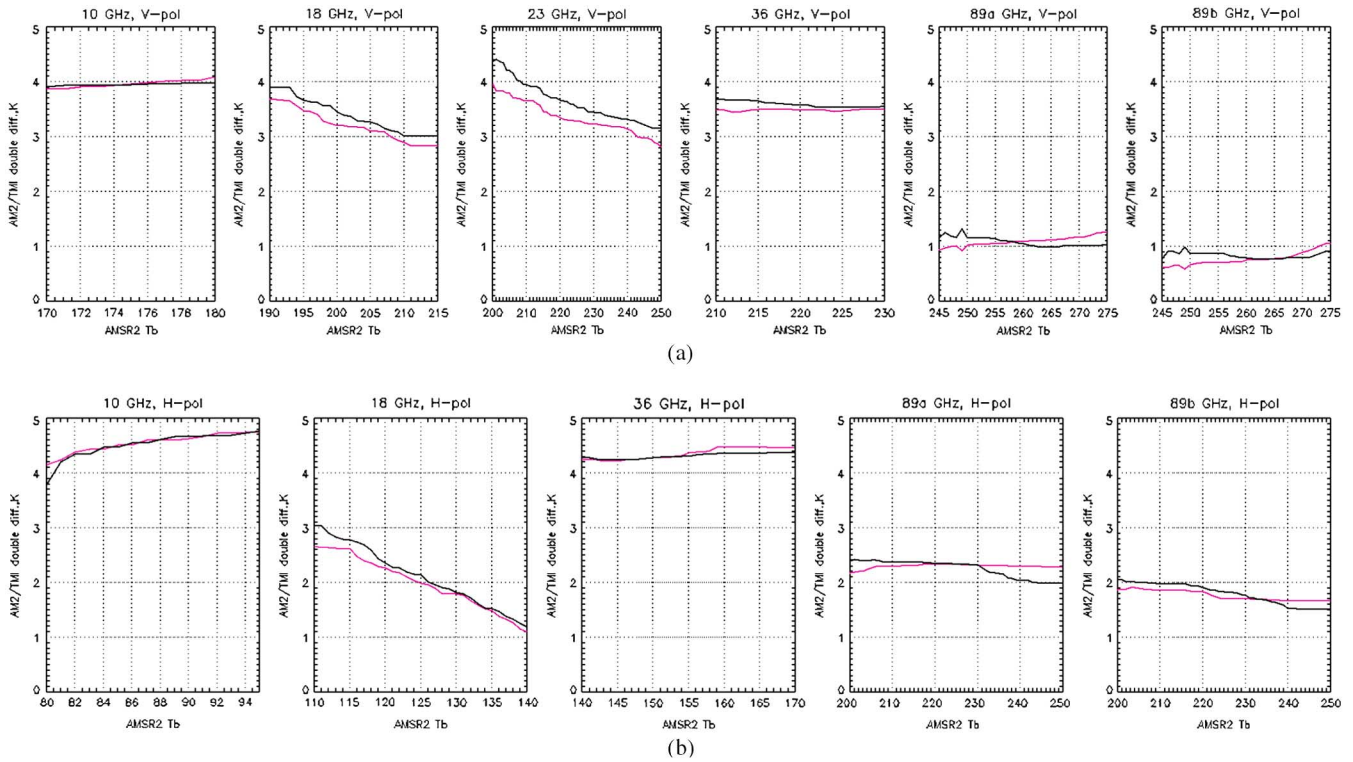


Fig. 4. Double difference as a function of AMSR2 measured (a) V-pol and (b) H-pol brightness temperatures. Red and black lines indicate results for ascending and descending satellite revolutions, respectively.

TABLE IV
AMSR2 MODELED DOUBLE DIFFERENCE EQUATION COEFFICIENTS

Channel	Ascending			Descending		
	a	b	c	a	b	c
10 GHz, V-pol	4.42×10^{-3}	-1.45	122.35	4.31×10^{-3}	-1.44	124.25
10 GHz, H-pol	2.02×10^{-3}	0.42	-16.35	4.78×10^{-3}	0.92	-39.67
18 GHz, V-pol	0.56×10^{-3}	-0.24	29.56	1.7×10^{-3}	-0.73	79.53
18 GHz, H-pol	6.47×10^{-5}	-0.07	9.79	0.55×10^{-3}	-0.20	18.10
23 GHz, V-pol	0.44×10^{-3}	-0.22	30.23	0.38×10^{-3}	-0.19	28.47
36 GHz, V-pol	1.33×10^{-3}	-0.57	64.27	1.66×10^{-3}	-0.71	80.48
36 GHz, H-pol	0.13×10^{-3}	-0.03	6.21	0.36×10^{-3}	-0.11	12.09
89a GHz, V-pol	2.77×10^{-3}	-1.41	181.26	3.43×10^{-3}	-1.76	227.10
89a GHz, H-pol	0.18×10^{-3}	-0.08	10.50	0.83×10^{-3}	-0.38	44.49
89b GHz, V-pol	3.27×10^{-3}	-1.66	212.41	3.51×10^{-3}	-1.79	229.40
89b GHz, H-pol	0.78×10^{-3}	-0.35	40.97	0.91×10^{-3}	-0.41	48.46

The discrepancies of direct comparison can be mitigated by calculating the SD using simulated Tbs from an RTM as described in Section III-B. The SD , defined in (1), minimizes the dynamic range of diurnal and seasonal cycle, and reduces the effect of EIA variability [25]

$$SD = Tb_{observed} - Tb_{simulated}. \quad (1)$$

The most important characteristic of the RTM is that it captures the dynamic change of the ocean scene radiance due

to changes in radiometer frequency, EIA, and polarization as well as changes in the environmental parameters. With the latter being derived from numerical weather models, they are imperfect estimates of the true values; hence, RTM can not exactly represent the physics of the observation. However, through the use of DD , the first-order RTM errors, which are linear with the relevant parameters will tend to cancel. Second-order errors will still show up in the DD analysis especially around the 23 GHz water vapor absorption line. These second-order errors can be mitigated by utilizing only clear-sky ocean scenes spanning long time periods for the calculation of the DD .

The DD , mathematically represented in (2), is calculated as the difference between the SD s of the two radiometers being inter-calibrated (AMSR2 and TMI in this study) on a channel-by-channel basis

$$DD_{Freq.,Pol} = SD_{Freq.,Pol}^{AMSR2} - SD_{Freq.,Pol}^{TMI}. \quad (2)$$

IV. AMSR2 INTER-CALIBRATION RESULTS

To perform AMSR2 inter-calibration with TMI, observations of the corresponding channels (frequency and polarization) from the two radiometers were collocated to establish a subset of ocean scenes (training dataset) that have homogeneous environmental conditions. For the training dataset, we used four months of collocated AMSR2 and TMI measurements (January to April, 2013), with a collocation criteria of 30 min maximum time difference, and 10 km maximum distance between the two sensors observations. The training dataset is then filtered for rain and clouds to assure rain-free clear-sky observations. TMI

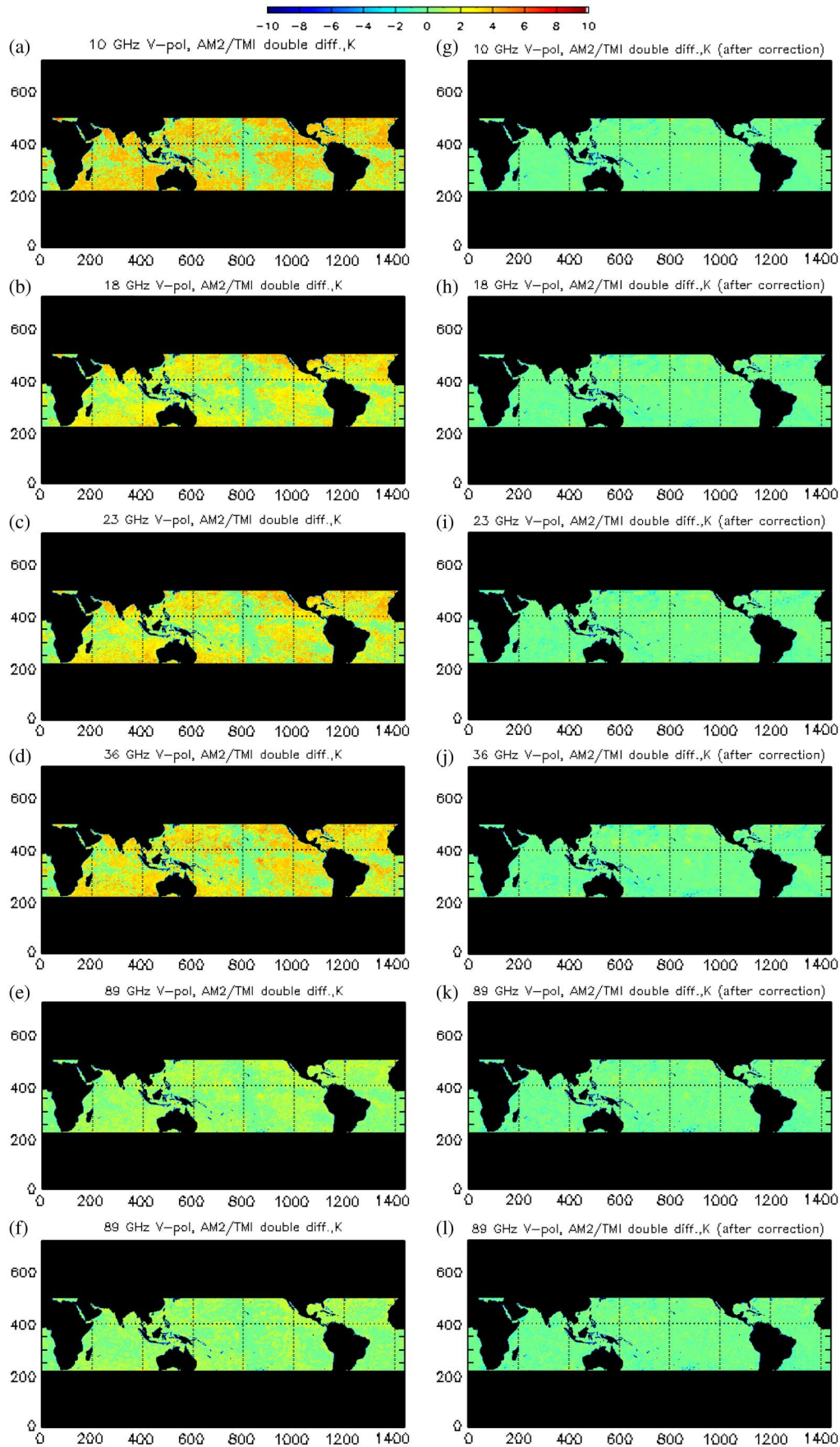


Fig. 5. V-pol double difference maps for (a) 10 GHz; (b) 18 GHz; (c) 23 GHz; (d) 36 GHz; (e) 89a GHz; and (f) 89b GHz. Left-side shows double difference maps before applying bias corrections to AMSR2 Tbs, and the right-side shows the double difference maps after applying bias corrections.

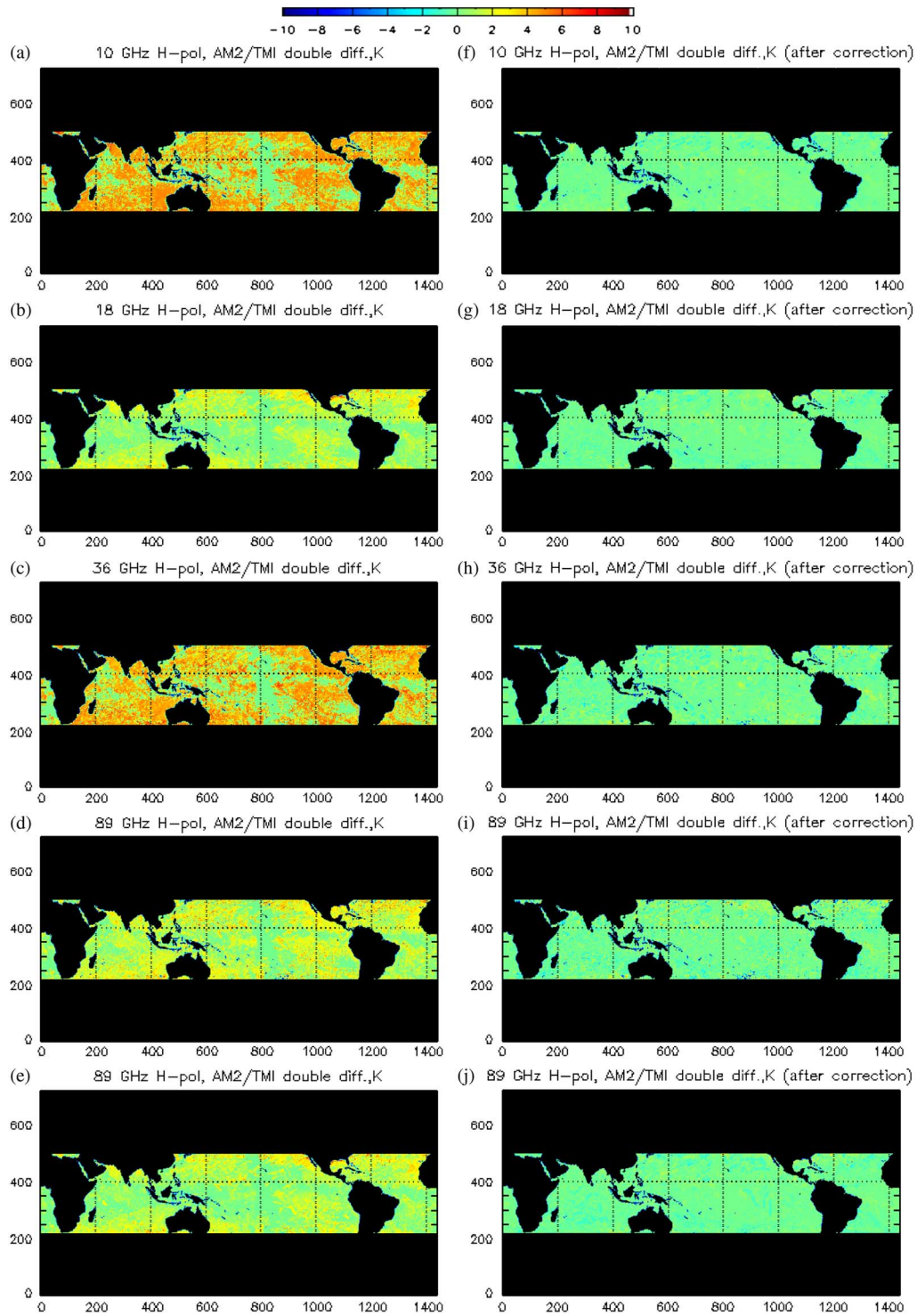


Fig. 6. H-pol double difference maps for (a) 10 GHz; (b) 18 GHz; (c) 36 GHz; (d) 89a GHz; and (e) 89b GHz. Left-side shows double difference maps before applying bias corrections to AMSR2 Tbs, and the right-side shows the double difference maps after applying bias corrections.

environmental daily retrieval maps (version 4) provided by Remote Sensing Systems were used for that purpose [26].

Next, as an additional quality control (*QC*) procedure, more stringent constraints were applied on all channels. First, all points with an absolute difference between observed and simulated Tbs > 5 K were excluded to remove outliers. A probable cause for these outliers is either they are rain contaminated observed Tbs, or erroneous simulated Tbs possibly due to unrealistic

modeled data. Second, if measured Tb values exceed the expected upper boundaries of brightness temperatures for rain-free ocean scenes, then these points were excluded from the training set. Third, AMSR2 ascending orbits are susceptible to significant sun glitter contamination. The additional QC procedure will eliminate these regions as much as possible using sun azimuth and elevation information provided in the L1B data files. Fig. 3 shows the difference between measured and simulated AMSR2

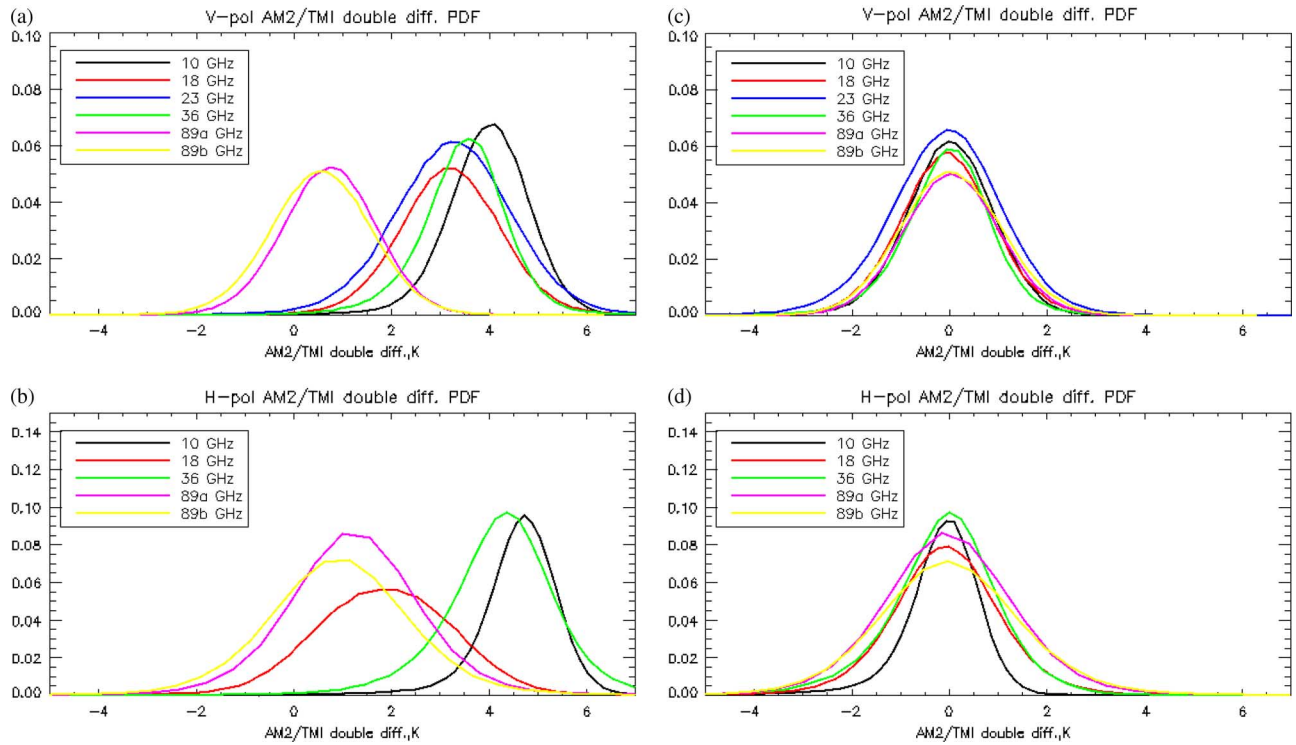


Fig. 7. AMSR2 double difference pdfs for (a) V-pol; (b) H-pol; (c) V-pol after applying bias corrections; and (d) H-pol after applying bias corrections.

Tbs (K) for the 6 GHz V-pol channel where sun glitter contaminated areas are encircled. Finally, an aggressive land mask is applied to remove any possible land contamination in the observed Tbs (100 km away from the coast).

Using the filtered training dataset (separated by frequency, polarization, and ascending/descending), the DD between AMSR2 and TMI was calculated as in (2). Table III shows the mean DD results for all AMSR2 channels with corresponding TMI counterparts. It clearly demonstrates that AMSR2 is measuring warmer Tbs than TMI.

Fig. 4 shows the binned and averaged DD (y-axis, K) with AMSR2 observed Tbs (x-axis, K), for all channels shown previously in Table III. In order to correct these biases, the DD was mathematically modeled as a function of AMSR2 Tbs on a channel-by-channel basis. A second-degree polynomial was used as shown in (3) to account for any possible nonlinearity in the biases

$$DD_{mod.} = ax^2 + bx + c \quad (3)$$

where $DD_{mod.}$ is the modeled DD , and x is the observed Tb for each channel. Coefficients a , b , and c needed to reconstruct corrections are shown in Table IV.

The modeled DD were then subtracted from AMSR2 measured Tbs ($Tb_{meas.}$) leading to corrected AMSR2 Tbs ($Tb_{cor.}$) as

$$Tb_{cor.} = Tb_{meas.} - DD_{mod.} \quad (4)$$

In order to validate AMSR2 Tb corrections, they were applied on an independent (not used to derive biases) validation dataset consisted of 1 month (June 2013) of AMSR2/TMI collocations. Figs. 5 and 6 demonstrate the DD maps for 10, 18, 23, 36, and 89 GHz V- and H-pol channels, respectively, averaged over the

validation dataset time period. The left-side panels show the DD maps before applying bias corrections to AMSR2 Tbs, where regions with warmer colors indicate the positive bias of AMSR2 Tbs. The right-side panels show the DD maps after applying bias corrections (homogeneous with around zero mean). It is worth mentioning that collocations with TMI are limited in latitude and to ocean scenes only, hence the black regions.

Moreover, Fig. 7 compares the probability density functions (pdfs) for AMSR2 DD results for both V- and H-pol channels. Left-side panels [Fig. 7(a) and (b)] show DD pdfs before applying bias corrections to AMSR2 Tbs, and the right-side panels [Fig. 7(c) and (d)] show the DD pdfs after applying bias corrections.

V. SENSOR STABILITY

To study the stability and consistency of AMSR2 measurements, we used the SD concept described in (1). However, since the calculation of the SD requires RTM to simulate Tbs using input parameters that are only an estimation of the true geophysical scene under observation, simulated Tbs may be erroneous. Therefore, SD by itself is not a good indicator for calibration errors, but it can be further analyzed to determine if the sensor of interest has any stability or consistency issues. This concept was successfully demonstrated for TMI solar bias correction [18], [19].

Thus for AMSR2, we calculated the SD from the training dataset and averaged the ocean SD for each day in that time period. Fig. 8 depicts a 4 months time series of the daily averaged oceanic SD values for all AMSR2 channels. No signs of instability (i.e., patterns in the SD plots) were shown in AMSR2 measurements based on this time period.

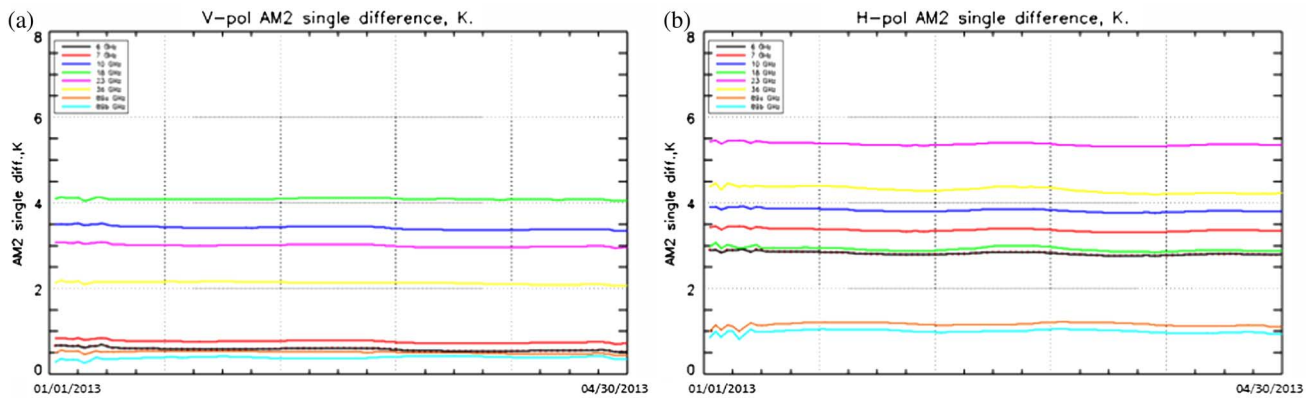


Fig. 8. Time series of AMSR2 daily averaged SD values for (a) V-pol channels and (b) H-pol channels.

VI. CONCLUSION

This study utilized 4 months of collocated AMSR2/TMI data to characterize AMSR2 biases with respect to TMI as the reference radiometer. The oceanic biases reported here are based on clear ocean scenes (filtered for rain and clouds) to minimize the *DD* discrepancies and maximize the robustness of the *DD* technique to estimate radiometric biases. In our analysis, L1B V1.1 and 1B11 V7 calibrated Tbs were used for AMSR2 and TMI, respectively.

Results revealed some rather significant residual calibration errors that still exist in AMSR2 Tb measurements (AMSR2 Tbs are ~ 2 to 4 K warmer than TMI). These biases were mathematically modeled and used in correcting AMSR2 observed brightness temperatures. The efficacy of the derived bias corrections was evaluated using an independent dataset filtered the same way as the training dataset. After applying bias corrections on AMSR2 Tbs, the double difference for all AMSR2 channels with corresponding TMI counterparts was with zero mean.

Moreover, AMSR2 self consistency was checked using the *SD* approach. The preliminary results based on 4 months of data show no patterns that can be correlated to sensor instability.

These oceanic AMSR2 Tb bias corrections are not intended to be extrapolated to correct AMSR2 observations over land scenes. Actually, corrected AMSR2 Tbs will be used in oceanic geophysical retrievals algorithms to infer higher-level environmental data products (e.g., sea surface temperature, sea surface wind speed, etc.), which will significantly improve the quality and accuracy of the retrieved geophysical parameters.

REFERENCES

- [1] N. C. Grody, "Remote sensing of atmospheric water content from satellites using microwave radiometry," *IEEE Trans. Antennas Propag.*, vol. 24, no. 2, pp. 155–162, Mar. 1976.
- [2] T. T. Wilheit and A. T. C. Chang, "An algorithm for retrieval of ocean surface and atmospheric parameters from the observations of the scanning multichannel microwave radiometer," *Radio Sci.*, vol. 15, pp. 525–544, 1980.
- [3] J. Hollinger, Ed., *DMSP Special Sensor Microwave Imager Calibration/Validation—Final Report*. Washington, DC, USA: Naval Research Laboratory, Jul. 1989.
- [4] J. Hollinger, J. Peirce, and G. Poe, "SSM/I instrument evaluation," *IEEE Trans. Geosci. Remote Sens.*, vol. 28, no. 5, pp. 781–790, Sep. 1990.
- [5] J. Hollinger, Ed., *DMSP Special Sensor Microwave Imager Calibration/Validation—Final Report*. Washington, DC, USA: Naval Research Laboratory, May 1991.
- [6] M. Colton and G. Poe, "Intersensor calibration of DMSP SSM/T's: F-8 to F-14, 1987–1997," *IEEE Trans. Geosci. Remote Sens.*, vol. 37, no. 1, pp. 418–439, Jan. 1999.
- [7] F. Wentz, "Inter-calibration of SSM/I F13, SSM/IS F16, and WindSat: A holistic approach (Invited)," *EOS Trans. AGU*, vol. 19, no. 26, 2010.
- [8] B. Yan and F. Weng, "Intercalibration between special sensor microwave imager/sounder and special sensor microwave imager," *IEEE Trans. Geosci. Remote Sens.*, vol. 46, no. 4, pp. 984–995, Apr. 2008.
- [9] F. Wentz, P. Ashcroft, and C. Gentemann, "Post-launch calibration of the TRMM microwave imager," *IEEE Trans. Geosci. Remote Sens.*, vol. 39, no. 2, pp. 415–422, Feb. 2001.
- [10] T. Meissner and F. Wentz, "Intercalibration of AMSR-E and Windsat brightness temperature measurements over land scenes," in *Proc. IEEE Int. Geosci. Remote Sens. Symp. (IGARSS)*, Jul. 2010, pp. 3218–3219.
- [11] S. Biswas *et al.*, "Intercalibration of microwave radiometer brightness temperatures for the global precipitation measurement mission," *IEEE Trans. Geosci. Remote Sens.*, vol. 51, no. 3, pp. 1465–1477, Mar. 2013.
- [12] "Overview of the Global Change Observation Mission (GCOM)," in *Proc. Int. Arch. Photogramm., Remote Sens. Spatial Inf. Sci.*, Kyoto, Japan, 2010, vol. 38, Part 8 [Online]. Available: http://www.isprs.org/proceedings/xxxviii/part8/pdf/JTS12_20100306153736.pdf
- [13] JAXA GCOM-W1 [Online]. Available: http://suzaku.eorc.jaxa.jp/GCOM_W/w_amsr2/whats_amsr2.html
- [14] K. Imaoka *et al.*, "Instrument performance and calibration of Amsr-E and Amsr2," in *Proc. Int. Arch. Photogramm. Remote Sens. Spat. Inf. Sci.*, Kyoto, Japan, 2010, vol. 38, Part 8.
- [15] *AMSR2 Level1 Product* [Online]. Available: ftp://suzaku.eorc.jaxa.jp/pub/AMSR2/public/Format/AMSR2_Level1_Product_Format_EN.pdf
- [16] *GCOM AMSR2 V1.1 Release* [Online]. Available: <https://gcom-w1.jaxa.jp/auth.html>
- [17] *GES DISC Webpage for TMI 1B11 Data* [Online]. Available: http://mirador.gsfc.nasa.gov/collections/TRMM_1B11_007.shtml
- [18] K. Gopalan *et al.*, "A time-varying radiometric bias correction for the TRMM microwave imager," *IEEE Trans. Geosci. Remote Sens.*, vol. 47, no. 11, pp. 3722–3730, Nov. 2009.
- [19] S. Biswas, K. Gopalan, W. Jones, and S. Bilanow, "Correction of time varying radiometric errors in TRMM microwave imager calibrated brightness temperature products," *IEEE Geosci. Remote Sens. Lett.*, vol. 7, no. 4, pp. 851–855, Oct. 2010.
- [20] *GES DISC Mirador Earth Science Data Search Tool* [Online]. Available: <http://mirador.gsfc.nasa.gov/>
- [21] Y. Han *et al.*, "JCSDA community radiative transfer model (CRTM)—Version 1," NOAA, Washington, DC, USA, Tech Rep. 122, 2006.
- [22] N. Bormann, A. Geer, and S. English, "Evaluation of the microwave ocean surface emissivity model FASTEM-5," IFS, ECMWF, Tech. Rep. 667, 2012.
- [23] A. Simmons, S. Uppala, D. Dee, and S. Kobayashi, "ERA-Interim: New ECMWF reanalysis products from 1989 onwards," *ECMWF Newsl.*, vol. 110, pp. 26–35, 2006.
- [24] J. Gibson *et al.*, "ECMWF Reanalysis Report Series 1—ERA Description," ECMWF, U.K., 1997, 72p. [Online]. Available: https://badc.nerc.ac.uk/data/ecmwf-era/era-15_doc.pdf

- [25] R. A. Kroodasma, D. S. McKague, and C. S. Ruf, "Inter-calibration of microwave radiometers using the vicarious cold calibration double difference method," *IEEE J. Sel. Topics Appl. Earth Observ. Remote Sens.*, vol. 5, no. 3, pp. 1006–1013, Jun. 2012.
- [26] *Remote Sensing Systems* [Online]. Available: <http://www.remss.com/missions/tmi>



Suleiman O. Alswiss (S'05–M'11) received the B.S. degree in electrical engineering from Princess Sumaya University for Technology, Amman, Jordan, in 2004, and the M.S. and Ph.D. degrees in electrical engineering from the University of Central Florida (UCF), Orlando, FL, USA, in 2007 and 2011, respectively.

From 2006 to 2011, he was a Research Assistant with the Central Florida Remote Sensing Laboratory (CFRSL), UCF, where his primary research focused on active and passive microwave remote sensing. In 2011, he joined NOAA/NESDIS/STAR, as a Support

Scientist with Global Science and Technology Inc. (GST), Greenbelt, MD, USA, where he continues his work in calibrating, developing, and validating satellite retrieval algorithms and products in an operational environment.



Zorana Jelenak (S'97–M'04) received the Ph.D. degree in physics from Waikato University, Hamilton, New Zealand, in 2000.

She joined as a UCAR Visiting Scientist with Ocean Winds Team, NOAA/NESDIS/ORA in March 2001, is a Member of the NASA Ocean Surface Winds Science Team, NOAA's EDR algorithm lead for AMSR-2 radiometer, and a Member of NASA CYGNSS Science Team. Her research interests include ocean surface wind vector measurements from active and passive microwave measurements and its

applicability in an operational near-real-time environment, retrieval algorithm development, model function development, advanced statistical analysis, and error analysis for improved algorithm characterization.



Paul S. Chang (S'87–M'90) received the B.S. degree in electrical engineering from the Union College, Schenectady, NY, USA, in 1988, and the Ph.D. degree in electrical engineering from the University of Massachusetts, Amherst, MA, USA, in 1994.

Since 1994, he has been a Research Physical Scientist with the Center for Satellite Applications and Research, National Environmental Satellite, Data, and Information Service (NESDIS), National Oceanic and Atmospheric Administration (NOAA), College Park, MD, USA, where he leads the NESDIS Ocean

Winds Science Team, is a Member of the NASA Ocean Surface Winds Science Team, and a Member of the NASA CYGNSS Science Team, and the Project Scientist for NOAA's GCOMW1 project. His research interests include research and development in active and passive microwave remote sensing of the ocean surface, with emphasis on retrieval of the ocean surface wind field. Wind retrieval algorithm improvements and new product developments are pursued through the analyses of satellite and aircraft microwave remote sensing data. An emphasis is placed on transitioning research results into operational use, which involves cooperative relationships with the operational facets of NESDIS and with the National Weather Service, a primary end user of these data. His current efforts are focused on working with international partners on the MetOp, Oceansat-2, and GCOM-W missions in addition to planning and risk reduction activities for future ocean vector wind missions.



Jun Dong Park (S'92–M'96–SM'05) received the B.S. degree from Konkuk University, Seoul, Korea, and the M.S. degree from the Florida Institute of Technology, Melbourne, FL, USA, both in electrical engineering, in 1993 and 1996, respectively.

He was a Research Associate with the Central Florida Remote Sensing Laboratory, University of Central Florida, Orlando, FL, USA. After he joined Northrop Grumman Mission Systems in 2005, he served DoD projects as a Senior Satellite Systems Engineer. Since 2007, he has been with Korean

Meteorological Administration to develop operational technique on Typhoon wind radii warning system using microwave and IR satellite remote sensor data, Global Precipitation Mission Ground Validation, and Communication, Ocean, and Meteorological Satellite (COMS) follow-on program. Currently, he is working as a Faculty Research Assistant with NOAA/NESDIS/CICS-UMD/ESSIC, College Park, MD, USA since March 2012 to develop GCOM/AMSR2 ocean EDR retrievals algorithm.



Patrick Meyers received the B.S. degree in atmospheric science from Cornell University, Ithaca, NY, USA, in 2008, and the M.S. degree in meteorology and physical oceanography from the Rosenstiel School of Marine and Atmospheric Science, University of Miami, Miami, FL, USA, in 2011.

From 2006 to 2008, he was a Summer Intern with the Gulf of Maine Research Institute, Portland, ME, USA. From 2011 to present, he has been a Faculty Research Assistant with the University of Maryland, College Park, MD, USA. His research interests

include passive microwave retrievals of precipitation.